RADIOPHYSICS

Original article
DOI: https://doi.org/10.18721/JPM.18414

NONDESTRUCTIVE TESTING OF OPTICAL FIBERS USING THE OPTICAL COHERENCE TOMOGRAPHY

Z. A. Erovenko[1], *A. A. Markvart*[1], *A. V. Petrov*[1], *M. A. Bisyarin*[2], *L. B. Liokumovich*[1], *N. A. Ushakov*✉[1]

[1] Peter the Great St. Petersburg Polytechnic University, St. Petersburg, Russia

[2] St. Petersburg State University, St. Petersburg, Russia

✉ n.ushakoff@spbstu.ru

Abstract. The paper presents a nonconventional approach to processing the interference signals of the optical coherence tomography (OCT) that allows for multiple improvements of the longitudinal spatial resolution of an image obtained. This technique is based on using the root-MUSIC spectral estimation algorithm. The parameters of this algorithm ensuring the accurate determination of the reflector coordinates within a sample have been found. In the course of the theoretical and numerical assessments carried out, the requirements for providing the superresolution by the root-MUSIC algorithm were defined and formulated. In order to evaluate the effectiveness of the proposed method experimentally, the cross-section geometric parameters of multimode and single-mode optical fibers were measured. The obtained results confirmed the validity of the approach that was put forward.

Keywords: optical fiber sensor, optical coherence tomography, root-MUSIC, superresolution; parametric spectral estimation

Funding: The reported study was funded by Russian Science Foundation (grant No. 23-72-10095), https://rscf.ru/project/23-72-10095/.

Citation: Erovenko Z. A., Markvart A. A., Petrov A. V., Liokumovich L. B., Ushakov N. A., Nondestructive testing of optical fibers using the optical coherence tomography, St. Petersburg State Polytechnical University Journal. Physics and Mathematics. 18 (4) (2025) 190–205. DOI: https://doi.org/10.18721/JPM.18414

Научная статья
УДК 681.785.57
DOI: https://doi.org/10.18721/JPM.18414

НЕРАЗРУШАЮЩИЙ КОНТРОЛЬ ОПТИЧЕСКИХ ВОЛОКОН С ПОМОЩЬЮ ОПТИЧЕСКОЙ КОГЕРЕНТНОЙ ТОМОГРАФИИ

З. А. Еровенко[1], А. А. Маркварт[1], А. В. Петров[1], М. А. Бисярин[2], Л. Б. Лиокумович[1], Н. А. Ушаков✉[1]

[1] Санкт-Петербургский политехнический университет Петра Великого, Санкт-Петербург, Россия

[2] Санкт-Петербургский государственный университет, Санкт-Петербург, Россия

✉ n.ushakoff@spbstu.ru

Аннотация. В работе представлен нетрадиционный подход к обработке интерференционных сигналов оптической когерентной томографияи (ОКТ), позволяющий добиться кратного улучшения ее продольной пространственной разрешающей способности. Предложенный метод основан на использовании алгоритма спектральной оценки root-MUSIC. Определены параметры этого алгоритма, **которые** обеспечивают нахождение координат отражателей внутри исследуемого образца. В ходе проведенных теоретических и численных оценок определены и сформулированы требования к обеспечению сверхразрешения алгоритмом root-MUSIC. Проверка эффективности предложенного метода проведена путем измерения геометрических параметров поперечных сечений многомодовых и одномодовых оптических волокон. Экспериментальные результаты подтвердили многократное улучшение пространственной разрешающей способности ОКТ.

Ключевые слова: волоконно-оптический датчик, оптическая когерентная томография, root-MUSIC, сверхразрешение, параметрическая оценка спектра

Финансирование: Исследование выполнено за счет гранта Российского научного фонда № 10095-72-23, https://rscf.ru/project/23-72-10095/.

Ссылка для цитирования: Еровенко З. А., Маркварт А. А., Петров А. В., Лиокумович Л. Б., Ушаков Н. А. Неразрушающий контроль оптических волокон с помощью оптической когерентной томографии // Научно-технические ведомости СПбГПУ. Физико-математические науки. 2025. Т. 18. № 4. С. 190–205. DOI: https://doi.org/10.18721/ JPM.18414

Introduction

Advances in photonics and its widespread adoption led to revolutionary transformations in various fields of science and technology, such as information and communication technologies, communication systems, sensor technologies for monitoring energy and construction facilities, as well as medical diagnostics. Optical fiber is an integral part of modern infrastructure, serving both as an information transmission medium and a sensing element in various devices. As great strides are made in photonics, there is a growing demand for nondestructive testing of components of fiber-optic systems for diagnostics and maintenance purposes; these systems include optical fibers in complex fiber-optic assemblies, as well as waveguides in photonic integrated circuits.

Optical reflectometers are often used as diagnostic tools for various optical waveguide structures [1]. However, they can only localize gross defects [2] and cannot visualize the defect, let alone a specific region of the fiber, for example, the splice between two fibers. Methods for preform diagnostics [3, 4] have a relatively low spatial resolution and are unsuitable for diagnosing

optical fibers without significant modification. Modern fiber-optic splicers can visualize the splice point only after splicing, however, the observed image is often qualitative and does not provide sufficient information to interpret the result in the case of splicing of different types of fibers.

Detailed visualization of the splice point in various fibers is crucial for development of fiber-optic sensors based on intermodal interferometers. Photonics methods are preferable for such visualization, as they can be integrated directly into the manufacturing process and there are no irreversible effects on the object under study.

Optical coherence tomography (OCT) [5] is an advanced experimental technique for studying various materials and transparent objects, providing three-dimensional images. OCT images are acquired from the so-called *A*-scans, representing the depth-resolved reflectivity profiles of the laser light backscattered from the sample. Moving the probe light beam over the sample surface and combining the obtained *A*-scans corresponding to different longitudinal sections of the sample yields 2D and 3D images (*B* and *C*-scans). Spectral-domain OCT (SD-OCT) has become widespread: in this case, *A*-scans are calculated as discrete Fourier transforms of spectral interference signals obtained from the interference of the reference wave with the scattered and backscattered light inside the sample.

The main application of OCT is biomedical diagnostics, which includes areas such as ophthalmology, endoscopic imaging, tissue characterization, and others [6]. A number of studies also applied this method for monitoring optical systems [7], testing semiconductor devices [8], and monitoring the additive manufacturing process [9]. Furthermore, OCT was used for measuring the core diameter in multimode optical fibers [10], which is often performed by other methods [11, 12].

As with any imaging device, the spatial resolution δz is an extremely important parameter for an OCT system. Since the longitudinal (in the direction of the probing beam propagation) and transverse (perpendicular to this direction) components of spatial resolution in OCT systems are determined by diverse factors, they can differ significantly, just as the methods for their improvement are different. The longitudinal component in SD-OCT depends on the spectral bandwidth $\Delta\lambda$ where the interference signal is measured [13]. The relationship of the longitudinal resolution with the parameters of the spectral band where the interference signal is measured is described by the expression

$$\Delta z = m(\lambda_0)^2/(2\Delta\lambda), \tag{1}$$

where λ_0 is the central wavelength of the spectral band used; m is the proportionality coefficient depending on the spectral shape of the light source (typically, $m \approx 1$).

Standard telecommunication optoelectronic components are the most common and accessible for implementing optical measuring systems operating in the spectral bands with central wavelengths of 1.30 and 1.55 μm. Typical tunable lasers and superluminescent diodes operating in these ranges provide spectral bandwidths up to 80–100 nm. Taking into account Eq. (1), the resulting longitudinal spatial resolution of such OCT systems can range from 8.5 to 15 μm. The requirements for spatial resolution for nondestructive testing of fiber-optic components and photonic integrated circuits are on the order of a few micrometers and less.

However, it is impossible to improve the resolution by simply increasing the spectral bandwidth $\Delta\lambda$, since the properties of available optical sources and the influence of chromatic dispersion of the material impose certain restrictions on this width [13, 14].

Acquisition of *A*-scans is equivalent to estimation of the spectrum of a polyharmonic signal. Therefore, various methods such as MUSIC and ESPRIT, capable of providing super-resolution [15–17], can improve the quality of OCT images. However, as shown in [18], the proposed improvement comes with some fundamental limitations related to the signal-to-noise ratio of the interference signal.

In this paper, we propose to increase the longitudinal spatial resolution of the SD-OCT system by using an improved signal processing technique.

The advantage of the proposed method is demonstrated by visualizing the cores of various optical fibers, including single-mode ones. The proposed approach can expand OCT to applications with requirements for high spatial resolution, for example, imaging of cell structures in biology, testing of photonic integrated circuits, and many others (some are currently even difficult to predict).

Interference signal processing for improved spatial resolution

The following model of the interference signal is used in this paper. The object under study is transparent, with no scattering centers distributed throughout its volume; the light inside the object is reflected from N interfaces between layers with different properties. Each jth layer is characterized by a refractive index n_j and a thickness L_j. When coherent waves backscattered within the sample undergo superposition with the high-intensity reference wave, interference occurs. If the reflections within the sample are assumed to be weak, the interference between the target waves can be neglected.

The spectral interference signal for the described model can be written as follows:

$$S(\lambda) = I_0 + \sum_{i=1}^{N} I_i + 2\sum_{i=1}^{N} \sqrt{I_0 I_i} \cos\left(2k \sum_{j=1}^{i} n_j L_j + \phi_i \right), \tag{2}$$

where n_j, L_j are the refractive index and the thickness of the jth layer, respectively; k is the wave number, $k = 2\pi/\lambda$; I_0, I_i are the intensities of the incident light and the light reflected from the ith interface; N is the number of interfaces; φ_i is the phase shift of the wave occurring upon reflection from the ith interface (equal to 0 or π for normal incidence and dielectric surfaces).

It should be borne in mind that the quantities I_i, n_i and φ_i may depend on the coherent radiation wavelength λ.

The purpose of OCT in this case is to estimate the internal structure of the object under study, namely, the optical distances $n_j \cdot L_j$. As follows from Eq. (2), the procedure for acquiring A-scans is equivalent to estimation of the polyharmonic signal spectrum. The simplest approach to performing such estimation is to calculate the discrete Fourier transform of the measured interference signal S. However, the longitudinal spatial resolution of OCT turns out to be limited by classical constraints described by Eq. (1).

On the other hand, it was shown in [19, 20] that spectral estimation methods such as the root-MUSIC algorithm can achieve super-resolution [15, 16] and, therefore, can improve the longitudinal spatial resolution of OCT. It was also found in [21] that the estimation errors of the root-MUSIC algorithm can approach the fundamental Cramer–Rao bound, making this method attractive for effective estimation of optical distances in OCT images.

Considering the signal described by Eq. (2) as a function of the light wavelength λ, the spatial frequencies ω_i of its interference components can be related to the optical path difference of the components OPD_i as follows:

$$\omega_i = k_0^2 \, \mathrm{OPD}_i / (2\pi), \tag{3}$$

where k_0 is the center of the wavenumber range where the spectral interference signal is measured.

Therefore, after estimating the spatial frequencies by the root-MUSIC algorithm, the OPD can be found as follows:

$$\mathrm{OPD}_i = L_i n_i = 2\pi\omega_i / k_0^2. \tag{4}$$

An important part of the root-MUSIC algorithm is to estimate the number of signal components of the target signal N, which is necessary in cases where this number is unknown. This estimate is typically obtained by analyzing the eigenvectors and eigenvalues of the covariance matrix of the processed signal using various information criteria [22–24], as well as empirical methods [17]. As a result of this analysis, the space of eigenvectors can be divided into two subspaces: signal and noise. If the dimension of the signal subspace N' is known, it is formed by eigenvectors corresponding to the largest eigenvalues.

However, in practice, the interference signal of OCT systems may contain a certain level of noise that can affect the accuracy of estimating the number of signal components. For this reason, it is necessary to investigate how the difference between the number of signal components N' set by the root-MUSIC algorithm and the true number of signal components N affects the accuracy of estimating the frequencies of the signal components.

For this purpose, we simulated a set of polyharmonic signals, randomly selecting such parameters as the number of signal components N, their frequencies f_i, amplitudes A_i, and the level of additive noise σ for each of them.

To control the complexity of the simulated signals, the maximum number of signal components did not exceed a certain preset value $N_{max} = 20$. The number of components in each generated signal was assumed to be a random variable with a uniform distribution from 1 to N_{max}.

The frequencies of the signal components were also assumed to be random variables with a uniform distribution from zero to half the sampling frequency f_S; the amplitudes obeyed a log-normal distribution with parameters $\mu = 0$ and $\sigma = 3$; the standard deviation of additive noise was assumed to be a random variable with a log-uniform distribution between 10^{-7} and 10^{-4}. The number of samples in the simulated signals was $M = 512$, which is close to practical values. The complete set consisted of 1,000 signals, each of which was characterized by random parameters.

To determine the errors in estimating the frequencies of the signal components by the root-MUSIC algorithm, we had to compare the frequencies found by this method with the frequencies of the signal components. If we assume that the signal-to-noise ratio (SNR) of the processed signal has a relatively high value and, consequently, the estimation errors of signal component frequencies are relatively small, then the problem of finding this correspondence can be formulated rather simply.

Specifically, it is necessary to calculate the matrix of squared residuals ΔF_{ie} between the true values of the frequencies f_i and their estimated values f'_e:

$$\Delta F_{ie} = (f_i - f'_e)^2. \quad (5)$$

The columns of matrix (5) correspond to the true values, and its rows correspond to the estimated values. We applied the Hungarian algorithm [25] to this matrix, making it possible to find the positions of certain elements of the matrix. The sum of these elements should be minimal, provided that only one element is selected from each row and column of this matrix. Since all the elements found were taken from unique rows and columns, thus minimizing the total error, the required correspondence between the simulated signal components and the estimated frequencies is guaranteed to be sufficiently accurate. The total error of frequency estimation (the sum of all matrix elements selected by the Hungarian algorithm) was used as a performance metric for the root-MUSIC algorithm under the given conditions.

The root-MUSIC method was used for all the simulated signals, so we obtained estimates of the frequencies of their components. The dimension of the signal space (serving as an important parameter of the root-MUSIC algorithm) varied in the range from 1 to $N_{max} = 20$. We should clarify that the number of components whose frequencies were estimated corresponded to the dimension of the signal space and had the maximum value N_{max}. Based on this, each signal was processed by the root-MUSIC algorithm, where the deviation ΔN of the estimated dimension of the signal subspace from the true one ($\Delta N = N' - N$) was varied over a certain range, with a maximum absolute deviation value of about $N_{max} = 20$. Fig. 1 shows the dependence $\Sigma[(\Delta f)^2]$ (ΔN), where Σ is the total squared estimation error for the frequencies of signal components $(\Delta f)^2$ by the root-MUSIC algorithm depending on the deviation ΔN of the estimated signal subspace dimension from the true one.

The obtained dependence is characterized by a lower error for deviations of the number of signal components $\Delta N < 0$, a sharp increase in error near $\Delta N = 0$, and then an almost constant level for $\Delta N > 0$. The reason for the relatively high error for $\Delta N > 0$ is that the sum of the squares of all errors is analyzed, and large frequency errors of individual components make a much greater contribution than the smaller ones.

When the deviation of the number of signal components ΔN turns out to be negative, the root-MUSIC algorithm identifies only the components with the largest amplitudes. Accordingly, these components had the highest signal-to-noise ratio (SNR) (since the noise level was the same for all frequency components in the same signal), producing the smallest errors. While root-MUSIC identified a larger number of components for ΔN values approaching zero, the amplitudes of the components and the SNR values decreased, resulting in increased frequency estimation errors manifested as a sharp rise in the total error. The sharp increase in error near

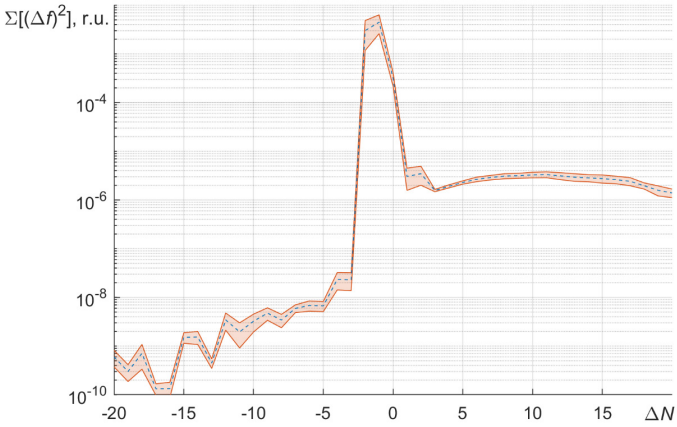

Fig. 1. Sum of squared estimation errors for frequencies of signal components $\Sigma[(\Delta f)^2]$ as a function of ΔN, the deviation of signal subspace dimension from the true one
Curves shown: mean error (dashed line) and standard deviation band (shaded colored region)

the point $\Delta N = 0$ suggests a potentially incorrect estimate of the signal component (its frequency may differ greatly from the true one) under the influence of noise. This indicates that in practical situations with a wide spread in amplitudes of the signal components, when there is a probability of low SNR values, it is preferable to slightly overestimate the signal subspace dimension if it is necessary to identify all the components. However, such a measure may require additional identification of the components to exclude false components and retain the correctly identified ones.

Additionally, we simulated the influence of signal subspace dimension on potential improvement in the longitudinal spatial resolution of OCT. The parameters of the numerical experiment were similar to those described above, the main differences were in a smaller number of interference components (there were only two of them). The amplitudes of the components were the same, and the frequency differences were varied from $0.05 f_S/M$ to $1.00 f_S/M$ (the quantity f_S/M converted to the OPD in Eq. (2) corresponds to the resolution limit for processing with FFT (see Eq. (1)). Numerical experiments were performed for three SNR values: 40, 60, and 80 dB. The dimension of the signal subspace was set equal to 2, 4, 10, 20, 50, 100, 200. Calculations for each combination of frequency difference of signal components, signal-to-noise ratios and signal subspace dimensions were repeated with 30 different noise realizations to estimate the standard deviation σ_f of the found signal component frequencies. If the difference between the

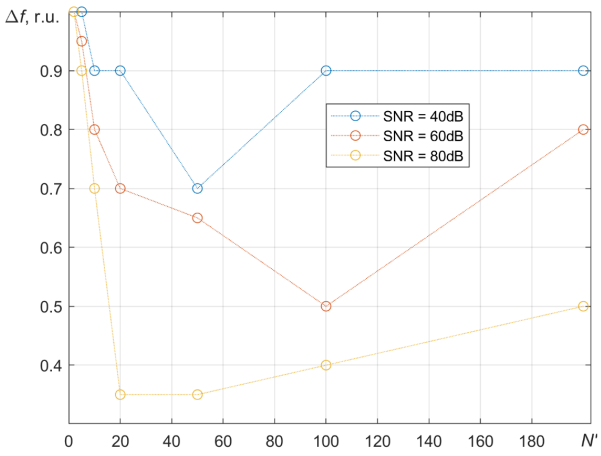

Fig. 2. Dependences of normalized frequency resolution for root-MUSIC algorithm on signal subspace dimension for different SNR values

true and found frequency values was less than σ_f, the root-MUSIC algorithm was deemed to perform satisfactorily. The smallest frequency difference Δf at which the root-MUSIC algorithm performed satisfactorily served as an estimate of the resolution achievable under these conditions. Fig. 2 shows the dependences of the normalized quantity $\Delta f/(f_s/M)$ on the signal subspace dimension N' for different SNR values.

As can be seen from the results of the numerical experiment, the optimal value of signal subspace dimension depends on SNR, however, values from 50 to 100 provide improved measurement resolution compared to processing with FFT for all SNR values at which the numerical experiment was conducted.

Experimental implementation of the method

Spectral interference signals were recorded with an NI PXIe-4844 optical sensor interrogator including a swept-wavelength laser and photodetectors. The optoelectronic module of the interrogator is similar to the Micron Optics si155-EV-04-1510-1590-0010-NO instrument, which has the following characteristics:

spectral range $\lambda = 1.51-1.59$ μm (central wavelength $\lambda_0 = 1.55$ μm, range width $\Delta\lambda = 80$ nm);

optical output power $P_0 = 60$ mW in each channel;

measurement frequency of interference signals equal to 10 Hz.

As established by our additional measurements [26], the noise equivalent power (NEP) of the photodetectors used in the interrogator is 80 pW in the entire operating bandwidth (about 1 MHz), the relative intensity noise (RIN) of the laser has a level of −50 dB over the entire frequency range.

The probe of the OCT system was a single-mode fiber optic patch cord with SMF-28 fiber. The probe was connected directly to one of the channels of the interrogator. A common-path OCT configuration was used, where reflection from the end face of the input fiber generates a reference wave reflected from the fiber/air interface. The interference of this reference wave with light waves backscattered from the irregularities of the object under study produces interference signals. Both the OCT probe and the fiber samples were mounted on Standa 7TF2 flexure stages ensuring micron positioning accuracy.

Evaluation of system performance

The noise level of the interference signal was estimated for the known parameters of the NI PXIe-4844 interrogator using the model from [27]. Neglecting the divergence of the light beam exiting the OCT probe and assuming that the three waves with the largest amplitudes, reflected from the glass/air interfaces (the end face of the OCT probe and both interfaces of the tested fiber) are the main factor affecting the intensity of the reflected waves, we can easily estimate the additive noise of the interference signal. Such noise is calculated as

$$\sigma_{add} \approx 3\, R_{\mathrm{F}a}\, P_0\, \mathrm{RIN} + \mathrm{NEP}, \tag{6}$$

where P_0 is the optical output power; RIN is the laser's relative intensity noise; NEP is the noise equivalent power of the photodetectors; $R_{\mathrm{F}a}$ is the Fresnel reflection coefficient at the glass/air interface.

The reflection coefficient follows the expression

$$R_{\mathrm{F}a} = [(n_{fiber} - n_{air}) / (n_{fiber} + n_{air})]^2, \tag{7}$$

where n_{fiber}, n_{air} are the refractive indices of fiber and air, respectively.

The value of $R_{\mathrm{F}a}$ in the spectral range of 1.55 μm is about 3.5%, which leads to an additive noise level $\sigma_{add} \approx 1.5$ nW.

To correctly estimate the amplitudes of the interference components, we should take into account the divergence of light waves, which is relatively difficult if the curvature of the reflecting surfaces and potential angular displacement are taken into account.

Thus, we deliberately overestimated the amplitudes of the interference components, because we neglected the divergence of the beam, since it is clear that in practice the amplitude values would be several times smaller.

The reflections at the core/cladding interface of the optical fiber tested are the weakest within the context of this study. The Fresnel reflection for single-mode fibers with a refractive index contrast of about 10^{-3} between the core and the cladding is $R_{cc} \approx 1.2 \cdot 10^{-7}$, which is five orders of magnitude less than the reflection from the fiber/air interface: $R_{Fa} \approx 0.035$.

If all of the above calculations are combined, it is possible to obtain an overestimated SNR value for the weakest interference component, which can be expressed as follows:

$$\mathrm{SNR} = [2 R_{cc} R_{Fa} (P_0)^2]/(\sigma_{add})^2. \quad (8)$$

For the parameters listed above, Eq. (8) leads to an estimated SNR of 10 dB for interference components generated by waves reflected from the interface between the core and the cladding. Unfortunately, the Cramer–Rao bounds for polyharmonic signals cannot be expressed explicitly, so they were calculated numerically in accordance with the procedure in [18]. The interference signal was assumed to have four interference components with the following amplitudes A_i and OPDs L_i:

$$A_1 = A_4 = 3.5 \text{ μW}, A_2 = A_3 = 6.5 \text{ nW},$$

$$L_1 = 30 \text{ μm}, L_2 = 115 \text{ μm}, L_3 = 127 \text{ μm}, L_4 = 212 \text{ μm}.$$

Under these conditions, the best achievable resolution for the estimated distance from the end of the OCT probe to the core/cladding interface is the value $\sigma_{Lcc} \approx 1.2$ nm.

Notably, several assumptions were made in the above reasoning, so the value of 1.2 nm may turn out to be an overly optimistic estimate. Furthermore, the value calculated above is a measure of the minimum detectable change in the distance from the OCT probe to the core/cladding interface rather than the spatial resolution, which characterizes the minimum difference in OPD of independently resolved interference components. Additionally, the best performance of the root-MUSIC algorithm is achieved in the case of a sufficiently large difference between the frequencies of the signal components, which can be determined by traditional processing methods, rather than in the super-resolution mode.

The above estimate of σ_{Lcc} can also be used to assess the presence of parasitic mechanical vibrations of the object considered. For this purpose, it is necessary to measure the displacement of the main reflectors, for example, by estimating the arguments of the main interference components, as often done in spectral interferometry and phase-sensitive OCT [28, 29]. If the level of measured vibrations significantly exceeds the value of σ_{Lcc}, compensation for parasitic vibrations should be carried out.

Measurement results

We measured the transverse profile of the reflection coefficient of coherent radiation for two fiber samples:

multimode fiber coated with a polymer layer and a step-index profile (Thorlabs FG050LGA);

SMF-28 single-mode fiber without coating.

Fig. 3. Schematic representation of mutual arrangement of test fiber and OCT probe (cross-sectional view): OCT system probe (OCT-SP); test fiber (TF). The vertical arrow indicates the direction in which the probe moves, the blue arrows indicate the direction of reflected light waves.

The relative arrangement of the probe and test fibers is schematically shown in Fig. 3. The optical fiber considered was mounted horizontally in the flexure stage, the OCT probe was also positioned horizontally, and the direction of the probe in the azimuthal plane was selected so that the amplitude of the observed interference signal was maximum. The interference signals were recorded while the OCT probe moved in the vertical

direction; the signals corresponded to different cross-sections of the fiber considered; this made it possible to visualize its cross-section as a two-dimensional scan (*B*-scan). The OCT probe moved with a step of 2 μm.

As established in the course of numerical simulation, a high SNR value of the processed signal is required for effective performance of the root-MUSIC algorithm. To improve the SNR in the conditions of our experimental setup, 200 interference signals were measured for each position of the OCT probe. Before applying the root-MUSIC algorithm, we first determined the phases of the principal interference components generated by waves reflected from the interfaces between the outer cladding of the optical fiber and the surrounding air. Next, we calculated the standard deviation of the position of the test fiber relative to the position of the OCT probe. In all cases, this deviation ranged from 1 to 2 nm, which is close to the OPD resolution $\sigma_{Lcc} \approx 1.2$ nm given above. This ratio indicated the absence of parasitic mechanical vibrations in the experimental setup.

The next step was to average the interference signals to improve the SNR value. All the results below were obtained with the signal subspace dimension in the root-MUSIC algorithm equal to 50. Excessive signal subspace dimension was chosen to achieve high resolution. Furthermore, because the object considered had a predictable structure, it was easy to identify any false signal components that the root-MUSIC method might yield.

A multimode fiber, with its high refractive index contrast and large core diameter, is the simplest structure to visualize in terms of OCT system requirements. Part of the *B*-scan of a multimode fiber with unremoved polymer coating is shown in Fig. 4,*a*. The image was obtained by applying FFT to interference signals; the backscattered signal intensity is represented by a color map. The interference signals processed by the root-MUSIC algorithm are represented by circles superimposed on an intensity map. Notice the large number of circles in the figure.

All spectral interferometry methods, including OCT, determine the OPD of interfering waves. Since the refractive index of quartz $n_{fiber} \approx 1.46$ differs from the refractive index of air $n_{air} \approx 1.00$, and it was important to determine the geometric parameters of the internal structure of quartz optical fibers in this work, the numerical values along the vertical axis were recalculated from the OPD by dividing by $n_{fiber} \approx 1.46$. Faint reflections at depths of about 320 and 800 μm correspond to the outer interfaces of the polymer coating, stronger reflections at depths of about 480 and 600 μm correspond to the interface between the fiber cladding and the polymer coating.

Analyzing the images in Fig. 4,*a*, we find that the fiber boundaries are clearly visible through the polymer coating, but the fiber core cannot be accurately identified due to strong backscattering of light inside the coating. Interference signals with *A*-scan numbers from 1800 to 1900 were averaged, leading to suppression of this backscattering due to its random nature. The *A*-scan obtained by this technique is shown in Fig. 5,*a*. Evidently, averaging suppresses the backscattering,

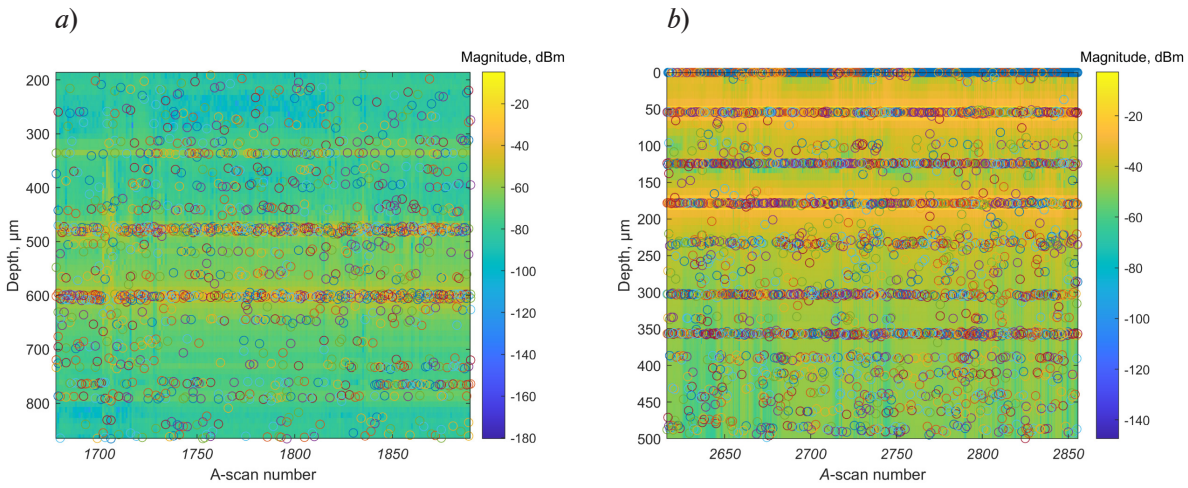

Fig. 4. Comparison of *B*-scans of multimode fiber with polymer coating (*a*) and single-mode fiber without coating (*b*):
calculated by FFT (intensity color maps) and the root-MUSIC algorithm with the signal subspace dimension of 50 (circles)

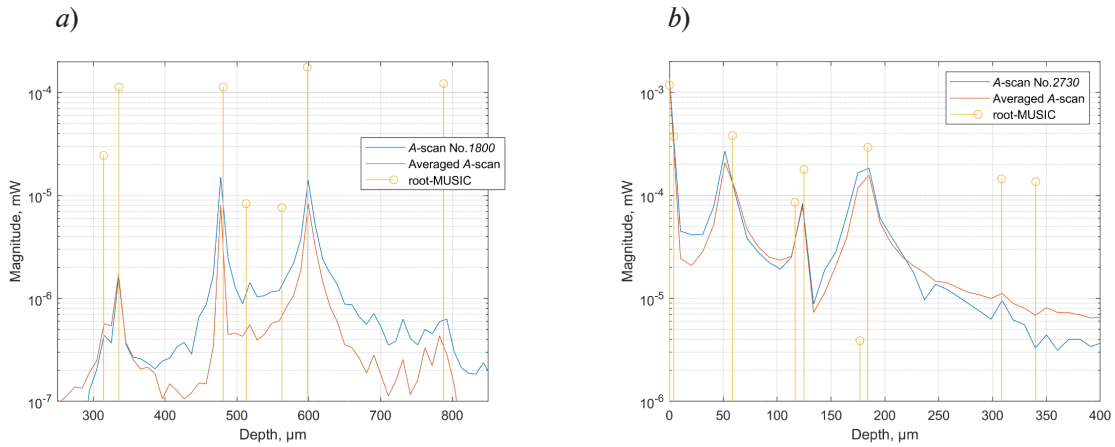

Fig. 5. Comparison of *A*-scans of multimode fiber with polymer coating (*a*) and single-mode fiber without coating (*b*): obtained for interference signals (IS) *1800* (*a*) and *2730* (*b*) (blue curves); for averaged IS with numbers from *1800* to *1900* (*a*) and with numbers from *2730* to *2830* (*b*) (red curves), as well as averaged IS processed by the root-MUSIC algorithm with signal subspace dimension equal to 50 (*a*,*b*) (vertical yellow lines)

making it possible to successfully identify the interfaces between the fiber core and the cladding using the root-MUSIC algorithm. Our estimate of the core diameter, which was 49.9 μm (based on the results of processing by the root-MUSIC algorithm), virtually coincides with its true value of 50.0 μm.

Similar measurements were performed for single-mode fiber. Fig. 4,*b* shows a fragment of a *B*-scan for the cross-section of standard single-mode SMF-28 fiber.

The same as for signals from multimode fiber, the image was obtained by applying FFT to interference signals, while the results of interference signal processing by the root-MUSIC algorithm are marked by circles. Reflections at depths of about 50 and 175 μm correspond to the surface of the fiber, reflections at a depth of about 130 μm correspond to the core/cladding interfaces. Analyzing the images in Fig. 4,*b*, we can also see that these interfaces cannot be resolved by classical FFT-based calculation of *A*-scans. To improve the SNR of the processed interference signal, we averaged the signals numbered from 2730 to 2830 next, the interference signal with improved SNR was processed by the root-MUSIC algorithm. The corresponding *A*-scans are compared in Fig. 5,*b*, showing the initial and averaged *A*-scans and the result of processing the latter by the root-MUSIC algorithm.

It should also be noted that the experimentally measured additive noise in the interference signals was 0.8 nW in the case of a single reflection from the OCT probe. When the light backscattered from the tested single-mode fiber was detected by the OCT probe, the level of additive noise reached 1.3 nW, which is very close to the analytical estimate of 1.5 nW. This slight discrepancy is most likely due to divergence of the light beam and, consequently, the lower proportion of laser intensity noise in the additive noise of the interference signal.

After averaging 100 interference signals, the total noise decreased from 1.30 to 0.15 nW. This indicates an almost complete lack of correlation between noise realizations, proving that averaging more signals can further improve the resolution, albeit at the cost of reduced measurement speed.

The amplitude of the interference components corresponding to the light waves reflected from the core/cladding interface of the single-mode fiber turned out to be close to 15 nW, providing an SNR value of about 17 dB, which was much higher than expected. An almost 10-fold improvement in the SNR value was required to resolve the two interference components, differing in OPD by 8 μm (which corresponds to 11.7 μm in air). This means that further research is necessary on the influence of the SNR value, parasitic modulation of interference components and the proximity of their location on the performance of the root-MUSIC algorithm (however, this is beyond the scope of this paper).

It should also be noted that the excessive signal subspace dimension used in the root-MUSIC algorithm made it possible to detect some spurious components caused by noise and imperfections in the experimental setup. For example, duplication of interference components at the fiber interfaces was caused by the circular shape of the optical fiber cross-section. Consequently, instead of a unique OPD between interfering waves, a variety of possible light paths that the reflected waves could travel existed, leading to a range of OPDs between the reflected and reference waves. This parasitic effect can be eliminated by optimizing the characteristics of the fiber OCT sensor, including focusing the output light beam. The overall performance of the OCT method may be improved by optimizing the parameters of the focusing lens for each individual measurement goal.

Conclusion

The paper proposes a new approach to nondestructive testing of the internal structure of optical fiber, which may be in high demand in the manufacturing of fiber-optic sensors, fiber-optic input/output couplers, as well as other components of fiber and integrated photonics.

We experimentally illustrated the approaches to visualizing the cores of both single-mode and multimode fibers coated with polymer layer thicker than 0.1 mm using optical coherence tomography and the root-MUSIC algorithm for acquiring *A*-scans.

An important feature of the proposed method is that it relies on relatively standard telecommunication optoelectronic components in the optical coherence tomography system.

The theoretical and numerical estimations were carried out to determine and formulate the requirements for ensuring super-resolution by the root-MUSIC algorithm. Furthermore, this algorithm for processing interference signals of optical coherence tomography can to automate the segmentation of the obtained images, simplify their interpretation, and, most importantly, improve spatial resolution.

The proposed approach is intended for visualizing the splices of single-mode and multimode fibers in the manufacturing of fiber-optic sensors based on intermodal interferometers. The problem is that interference signals from such sensors often differ from those predicted theoretically. The most promising method for solving the problem is to optimize the splicing mode of two different fibers, which can be achieved by obtaining quantitative information about the distribution of the refractive index of these fibers at the splices.

REFERENCES

1. **Lobach I. A., Fotiadi A. A., Yatseev V. A., et al.,** Newest methods and approaches to enhance the performance of optical frequency-domain reflectometers, Sensors. 24 (16) (2024) 5432.

2. **Ponomarev R. S., Konstantinov Yu. A., Belokrylov M. E., et al.,** An automated instrument for reflectometry study of the pyroelectric effect in proton-exchange channel waveguides based on lithium niobate, Instrum. Exp. Tech. 65 (5) (2022) 787–796.

3. **Konstantinov Y. A., Turov A. T., Latkin K. P., et al.,** A non-destructive study of optical, geometric and luminescent parameters of active optical fibers preforms, Optics. 5 (1) (2024) 176–194.

4. **Vladimirova D., Pervadchuk V., Konstantinov Y.,** Manufacture of microstructured optical fibers: Problem of optimal control of silica capillary drawing process, Comput. 12 (5) (2024) 86.

5. **Podoleanu A. G.,** Fiber optics, from sensing to non invasive high resolution medical imaging, J. Light. Technol. 28 (4) (2010) 624– 640.

6. **Fujimoto J., Swanson E.,** The development, commercialization, and impact of optical coherence tomography, Invest. Ophthalmol. Vis. Sci. 57 (9) (2016) OCT1 – OCT13.

7. **Gong Zh., Yu Ch., Guo D., et al.,** Three-dimensional optical coherence digital-null deformography of multi-refractive-surface optics with nanometer sensitivity, Opt. Express. 30 (23) (2022) 42069–42085.

8. **Ozaki N., Ishida K., Nishi T., et al.,** OCT with a visible broadband light source applied to high-resolution nondestructive inspection for semiconductor optical devices (Chapter 10), In book: M. R. Wang (Editor). "Optical coherence tomography and its non-medical applications", IntechOpen, 2020. Available from: http://dx.doi.org/10.5772/int.

9. **Opitz J., Porstmann V., Schreiber L., et al.,** Optical coherence tomography as monitoring technology for the additive manufacturing of future biomedical parts, In book: Meyendorf N., Ida N., Singh R., Vrana J. (Eds.). "Handbook of nondestructive evaluation 4.0". Springer International Publishing, Cham, Switzerland (2022) 859– 881.

10. **Saccon F. A. M., Muller M., Fabris J. L.,** Optical fiber characterization by optical coherence tomography, Proc. Int. Microwave and Optoelectronics Conf. (IMOC 2009). 3–6 Nov. 2009. Belem, Brazil (2009) 625–628.

11. **Henao R. H., Pomarico J. A., Russo N. A., et al.,** Multimode optical fiber core measurement by speckle correlation, Opt. Eng. 35 (1) (1996) 26–30.

12. **Golnabi H.,** Fiber core size determination from power measurements in a fiber-to-fiber design, Microwave Opt. Technol. Lett. 53 (6) (2011) 1225–1229.

13. **Drexler W.,** Ultrahigh-resolution optical coherence tomography, J. Biomed. Opt. 9 (1) (2004) 47–74.

14. **Ushakov N. A., Makovetskaya T. A., Markvart A. A., Liokumovich L. B.,** Theoretical foundations of quantum spectral-domain optical coherence tomography with frequency scanning, JETP Lett. 117 (1) (2023) 24–31.

15. **Li Y., Zhao K., Zhao J., et al.,** Super-resolution demodulation for fiber sensor arrays based on the MUSIC algorithm, Opt. Lett. 47 (10) (2022) 2390–2393.

16. **Langoju R., Patil A., Rastogi P.,** Super-resolution Fourier transform method in phase shifting interferometry, Opt. Express. 13 (18) (2005) 7160–7173.

17. **Ushakov N., Markvart A., Liokumovich L.,** Singlemode-multimode-singlemode fiber-optic interferometer signal demodulation using MUSIC algorithm, Photonics. 9 (11) (2022) 879.

18. **Rife D. C., Boorstyn R. R.,** Multiple tone parameter estimation from discrete time observations, Bell Syst. Tech. J. 55 (9) (1976) 1389–1410.

19. **Schmidt R. O.,** Multiple emitter location and signal parameter estimation, IEEE Trans. Antennas Propag. 34 (3) (1986) 276–280.

20. **Rao B. D., Hari K. V. S.,** Performance analysis of Root-Music, IEEE Trans. Acoust. Speech Signal Process. 37 (12) (1989) 1939–1949.

21. **Stoica P., Nehorai A.,** MUSIC, maximum likelihood, and Cramйr-Rao bound: further results and comparisons, IEEE Trans. Acoust. Speech Signal Process. 38 (12) (1990) 2140–2150.

22. **Wax M., Kallath T., Kailath T.,** Detection of signals by information theoretic criteria, IEEE Trans. Acoust. Speech Signal Process. 33 (2) (1985) 387–392.

23. **Zhao L. C., Krishnaiah P. R., Bai Z. D.,** On detection of the number of signals in presence of white noise, J. Multivar. Anal. 20 (1) (1986) 1–25.

24. **Stoica P., Selen Y.,** Model-order selection, IEEE Signal Process. Mag. 21 (4) (2004) 36–47.

25. **Munkres J.,** Algorithms for the assignment and transportation problems, SIAM J. Appl. Math. 5 (1) (1957) 32–38.

26. **Ushakov N. A., Markvart A. A., Liokumovich L. B.,** Enhancing the resolution limits of spectral interferometric measurements with swept-wavelength interrogation by means of a reference interferometer, Appl. Opt. 54 (19) (2015) 6029–6036.

27. **Ushakov N. A., Liokumovich L. B.,** Resolution limits of extrinsic Fabry –Perot interferometric displacement sensors utilizing wavelength scanning interrogation, Appl. Opt. 53 (23) (2014) 5092–5099.

28. **Ushakov N. A., Markvart A. A., Liokumovich L. B.,** Pulse wave velocity measurement with multiplexed fiber optic Fabry – Perot interferometric sensors, IEEE Sens. J. 20 (19) (2020) 11302–11312.

29. **Li P., Shen T. T., Johnstone M., Wang R. K.,** Pulsatile motion of the trabecular meshwork in healthy human subjects quantified by phase-sensitive optical coherence tomography, Biomed. Opt. Express. 4 (10) (2013) 2051.

СПИСОК ЛИТЕРАТУРЫ

1. **Lobach I. A., Fotiadi A. A., Yatseev V. A., Konstantinov Y. A., Barkov F. L., Claude D., Kambur D. A., Belokrylov M. E., Turov A. T., Korobko D. A.** Newest methods and approaches to enhance the performance of optical frequency-domain reflectometers // Sensors. 2024. Vol. 24. No. 16. P. 5432.

2. **Пономарев Р. С., Константинов Ю. А., Белокрылов М. Е., Шевцов Д. И., Карнаушкин П. В.** Автоматизированный инструмент рефлектометрического исследования пироэлектрического эффекта в протонообменных канальных волноводах на основе ниобата лития // Приборы и техника эксперимента. 2022. Т. 65. № 5. С. 96–106.

3. **Konstantinov Y. A., Turov A. T., Latkin K. P., Claude D., Azanova I. S.** A non-destructive study of optical, geometric and luminescent parameters of active optical fibers preforms // Optics. 2024. Vol. 5. No. 1. Pp. 176–194.

4. **Vladimirova D., Pervadchuk V., Konstantinov Y.** Manufacture of microstructured optical fibers: Problem of optimal control of silica capillary drawing process // Computation. 2024. Vol. 12. No. 5. P. 86.

5. **Podoleanu A. G.** Fiber optics, from sensing to non invasive high resolution medical imaging // Journal of Lightwave Technology. 2010. Vol. 28. No. 4. Pp. 624– 640.

6. **Fujimoto J., Swanson E.** The development, commercialization, and Impact of optical coherence tomography // Investigative Ophthalmology & Visual Science. 2016. Vol. 57. No. 9. Pp. OCT1 – OCT13.

7. **Gong Zh., Yu Ch., Guo D., Ding Zh., Li P.** Three-dimensional optical coherence digital-null deformography of multi-refractive-surface optics with nanometer sensitivity // Optics Express. 2022. Vol. 30. No. 23. Pp. 42069–42085.

8. **Ozaki N., Ishida K., Nishi T., Ohsato H., Watanabe E., Ikeda N., Sugimoto Y.** OCT with a visible broadband light source applied to high-resolution nondestructive inspection for semiconductor optical devices (Chapter 10) // M. R. Wang (Editor). “Optical coherence tomography and its non-medical applications”. USA: IntechOpen, 2020. Available from: http://dx.doi.org/10.5772/int

9. **Opitz J., Porstmann V., Schreiber L., et al.** Optical coherence tomography as monitoring technology for the additive manufacturing of future biomedical parts // Meyendorf N., Ida N., Singh R., Vrana J. (Eds.). “Handbook of nondestructive evaluation 4.0”. Cham, Switzerland: Springer International Publishing, 2022. Pp. 859– 881.

10. **Saccon F. A. M., Muller M., Fabris J. L.** Optical fiber characterization by optical coherence tomography // Proceedings of the International Microwave and Optoelectronics Conference (IMOC 2009). 3–6 November, 2009. Belem, Brazil. Pp. 625–628.

11. **Henao R. H., Pomarico J. A., Russo N. A., Torroba R., D., Trivi M.** Multimode optical fiber core measurement by speckle correlation // Optical Engineering. 1996. Vol. 35. No. 1. Pp. 26–30.

12. **Golnabi H.** Fiber core size determination from power measurements in a fiber-to-fiber design // Microwave and Optical Technology Letters. 2011. Vol. 53. No. 6. Pp. 1225–1229.

13. **Drexler W.** Ultrahigh-resolution optical coherence tomography // Journal of Biomedical Optics. 2004. Vol. 9. No. 1. Pp. 47–74.

14. **Ушаков Н. А., Маковецкая Т. А., Маркварт А. А., Лиокумович Л. Б.** Теоретические основы квантовой спектральной оптической когерентной томографии с частотным сканированием // Письма в ЖЭТФ. 2023. Т. 117. № 1. С. 29–36.

15. **Li Y., Zhao K., Zhao J., Wang J., Wright R., Buric M., Chen K. P.** Super-resolution demodulation for fiber sensor arrays based on the MUSIC algorithm // Optics Letters. 2022. Vol. 47. No. 10. Pp. 2390–2393.

16. **Langoju R., Patil A., Rastogi P.** Super-resolution Fourier transform method in phase shifting interferometry // Optics Express. 2005. Vol. 13. No. 18. Pp. 7160–7173.

17. **Ushakov N., Markvart A., Liokumovich L.** Singlemode-multimode-singlemode fiber-optic interferometer signal demodulation using MUSIC algorithm // Photonics. 2022. Vol. 9. No. 11. P. 879.

18. **Rife D. C., Boorstyn R. R.** Multiple tone parameter estimation from discrete time observations // Bell System Technical Journal. 1976. Vol. 55. No. 9. Pp. 1389–1410.

19. **Schmidt R. O.** Multiple emitter location and signal parameter estimation // IEEE Transactions on Antennas and Propagation. 1986. Vol. 34. No. 3. Pp. 276–280.

20. **Rao B. D., Hari K. V. S.** Performance analysis of Root-Music // IEEE Transactions on Acoustics, Speech, and Signal Processing. 1989. Vol. 37. No. 12. Pp. 1939 –1949.

21. **Stoica P., Nehorai A.** MUSIC, maximum likelihood, and Cramйr-Rao bound: further results and comparisons // IEEE Transactions on Acoustics, Speech, and Signal Processing. 1990. Vol. 38. No. 12. Pp. 2140–2150.

22. **Wax M., Kallath T., Kailath T.** Detection of signals by information theoretic criteria // IEEE Transactions on Acoustics, Speech, and Signal Processing. 1985. Vol. 33. No. 2. Pp. 387–392.

23. **Zhao L. C., Krishnaiah P. R., Bai Z. D.** On detection of the number of signals in presence of white noise // Journal of Multivariate Analysis. 1986. Vol. 20. No. 1. Pp. 1–25.

24. **Stoica P., Selen Y.** Model-order selection // IEEE Signal Processing Magazine. 2004. Vol. 21. No. 4. Pp. 36–47.

25. **Munkres J.** Algorithms for the assignment and transportation problems // Journal of the Society for Industrial and Applied Mathematics. 1957. Vol. 5. No. 1. Pp. 32–38.

26. **Ushakov N. A., Markvart A. A., Liokumovich L. B.** Enhancing the resolution limits of spectral interferometric measurements with swept-wavelength interrogation by means of a reference interferometer // Applied Optics. 2015. Vol. 54. No. 19. Pp. 6029–6036.

27. **Ushakov N. A., Liokumovich L. B.** Resolution limits of extrinsic Fabry –Perot interferometric displacement sensors utilizing wavelength scanning interrogation // Applied Optics. 2014. Vol. 53. No. 23. Pp. 5092–5099.

28. **Ushakov N. A., Markvart A. A., Liokumovich L. B.** Pulse wave velocity measurement with multiplexed fiber optic Fabry – Perot interferometric sensors // IEEE Sensors Journal. 2020. Vol. 20. No. 19. Pp. 11302–11312.

29. **Li P., Shen T. T., Johnstone M., Wang R. K.** Pulsatile motion of the trabecular meshwork in healthy human subjects quantified by phase-sensitive optical coherence tomography // Biomedical Optics Express. 2013. Vol. 4. No. 10. P. 2051.

THE AUTHORS

EROVENKO Zoya A.
Peter the Great St. Petersburg Polytechnic University
29 Politechnicheskaya St., St. Petersburg, 195251, Russia
zoya199306@gmail.com
ORCID: 0000-0002-9196-8038

MARKVART Aleksandr A.
Peter the Great St. Petersburg Polytechnic University
29 Politechnicheskaya St., St. Petersburg, 195251, Russia
markvart_aa@spbstu.ru
ORCID: 0000-0001-8080-0830

PETROV Aleksandr V.
Peter the Great St. Petersburg Polytechnic University
29 Politechnicheskaya St., St. Petersburg, 195251, Russia
alexandr-petroff1994@yandex.ru
ORCID: 0000-0001-5216-6588

BISYARIN Mikhail A.
St. Petersburg State University
7–9 Universitetskaya Emb., St. Petersburg, 199034, Russia
m.bisyarin@spbu.ru
ORCID: 0000-0003-3891-1339

LIOKUMOVICH Leonid B.
Peter the Great St. Petersburg Polytechnic University
29 Politechnicheskaya St., St. Petersburg, 195251, Russia
leonid@spbstu.ru
ORCID: 0000-0001-5988-1429

USHAKOV Nikolai A.
Peter the Great St. Petersburg Polytechnic University
29 Politechnicheskaya St., St. Petersburg, 195251, Russia
n.ushakoff@spbstu.ru
ORCID: 0000-0002-3480-2779

СВЕДЕНИЯ ОБ АВТОРАХ

ЕРОВЕНКО Зоя Андреевна – *ассистент Высшей школы прикладной физики и космических технологий Санкт-Петербургского политехнического университета Петра Великого.*
195251, Россия, г. Санкт-Петербург, Политехническая ул., 29
zoya199306@gmail.com
ORCID: 0000-0002-9196-8038

МАРКВАРТ Александр Александрович – *кандидат физико-математических наук, доцент Высшей школы прикладной физики и космических технологий Санкт-Петербургского политехнического университета Петра Великого.*
195251, Россия, г. Санкт-Петербург, Политехническая ул., 29
markvart_aa@spbstu.ru
ORCID: 0000-0001-8080-0830

ПЕТРОВ Александр Викторович – *кандидат физико-математических наук, доцент Высшей школы прикладной физики и космических технологий Санкт-Петербургского политехнического университета Петра Великого.*
195251, Россия, г. Санкт-Петербург, Политехническая ул., 29
alexandr-petroff1994@yandex.ru
ORCID: 0000-0001-5216-6588

БИСЯРИН Михаил Александрович – *доктор физико-математических наук, ведущий научный сотрудник кафедры радиофизики Санкт-Петербургского государственного университета.*
199034, Россия, г. Санкт-Петербург, Университетская наб.,7–9
bisyarin@spbu.ru
ORCID: 0000-0003-3891-1339

ЛИОКУМОВИЧ Леонид Борисович – *доктор физико-математических наук, профессор Высшей школы прикладной физики и космических технологий Санкт-Петербургского политехнического университета Петра Великого.*
195251, Россия, г. Санкт-Петербург, Политехническая ул., 29
leonid@spbstu.ru
ORCID: 0000-0001-5988-1429

УШАКОВ Николай Александрович – *доктор физико-математических наук, профессор Высшей школы прикладной физики и космических технологий Санкт-Петербургского политехнического университета Петра Великого.*
195251, Россия, г. Санкт-Петербург, Политехническая ул., 29
n.ushakoff@spbstu.ru
ORCID: 0000-0002-3480-2779

Received 02.05.2025. Approved after reviewing 14.05.2025. Accepted 14.05.2025.
Статья поступила в редакцию 02.05.2025. Одобрена после рецензирования 14.05.2025. Принята 14.05.2025.